J. Plasma Physics (2006), *vol.* 72, *part* 1, *pp.* 11–33. © 2005 Cambridge University Press
doi:10.1017/S002237780500379X first published online 25 Nov. 2005 Printed in the United Kingdom

Interaction of electromagnetic waves with a radially bounded electron beam

C. KRAFFT[1], B. LUNDIN[2] and A. VOLOKITIN[2]

[1]Laboratoire de Physique des Gaz et des Plasmas, Université Paris-Sud, 91405 Orsay Cedex, France
(catherine.krafft@pgp.u-psud.fr)

[2]Institute of Terrestrial Magnetism, Ionosphere and Radiowave Propagation, Russian Academy of Sciences, Troitsk, Moscow Region, 142190, Russia

(Received 1 November 2004 and in revised form 1 November 2004; accepted 10 December 2004)

Abstract. The resonant interaction of a narrow electron beam spiraling in a cold homogeneous magnetized plasma with electromagnetic cylindrical waves is considered. The conclusions derived in recent papers about the formation, in the presence of effective electromagnetic energy dissipation out of the radially bounded beam, of dynamically stable and longtime living bunches of resonant electrons in the developed stage of their nonlinear interaction with the waves are discussed in this paper for more general physical cases and for wider ranges of characteristic parameters. General analytical formulas for the excited electromagnetic fields, the radiated electromagnetic power flux and the linear growth rate as well as relevant numerical simulations results are presented.

1. Introduction

The linear and nonlinear interactions of energetic particles' beams with electromagnetic waves in magnetized plasmas are the subject of many theoretical papers and numerical simulations since several decades (see, for example, [1–29] and references therein). They were mainly motivated by the numerous laboratory and space experiments involving electron beam injection and by the observations of natural suprathermal particles' streams travelling in planetary, solar and astrophysical plasmas (see [30–48] and references therein). Up to now, the plasma processes involving the participation of localized currents or particles' beams remain a subject at the forefront of research on natural or artificially induced plasma phenomena, in space and in laboratory.

In recent papers devoted to the investigation of the nonlinear stage of the resonant interaction of a radially bounded modulated electron beam with low-frequency waves in a homogeneous magnetized plasma [22–29], the crucial influence of the wave energy leakage out of the beam volume across the ambient magnetic field on the features of the wave–particle interaction processes was clearly demonstrated and interpreted. A new nonlinear process was pointed out which consists in the self-organization of the beam structure through the formation of electron bunches continuously accelerated or decelerated by the waves, depending on what beam–wave resonance conditions are considered. The presence of energy leakage allows

https://doi.org/10.1017/S002237780500379X Published online by Cambridge University Press

the appearance of dynamically stable electron bunches and, when a large number of waves are considered, leads to competition between the quasi-linear beam relaxation and the beam bunching, resulting in the possibility for the beam to radiate electromagnetic energy up to a significant distance from the injector. The specificity of the approach used by Volokitin, Krafft and coworkers [22–29] consists of a semi-analytical treatment: after the theoretical determination of the wave fields as functions of a given electron-beam current distribution, the full nonlinear dynamics of the electrons moving in the background magnetic and the wave fields are calculated numerically.

However, up to now, the investigation of this problem was performed for the case of sheared whistlers (whistler waves with perpendicular wave numbers essentially exceeding the parallel wave number, in the frequency domain where the electron gyrofrequency ω_c is much greater than the wave frequency ω) or lower hybrid waves only, which allowed essential simplifications of the Maxwell equations and reduced the computer resources meanwhile providing new and clear interpretable results. The present study gives the possibility to extend the investigation of the wave–beam interaction to wider ranges of physical parameters: actually a larger wave frequency domain is covered for whistlers and the obtained formulas are applicable for any cold plasma mode. This namely allows one to investigate the interaction of whistler waves and beam particles in plasma depletion regions where $\omega_p \lesssim \omega_c$ (ω_p is the electron plasma frequency), which is, for example, typical of wide domains of the terrestrial ionosphere at heights around 1000–2000 km (e.g. [49]) or of the auroral magnetosphere in space regions of plausible generation of the so-called Auroral Kilometer Radiation [50].

At a given beam modulation frequency and parallel beam velocity, two whistler waves (or branches) of the same parallel wave number k_z, satisfying to the same Landau or cyclotron resonance conditions but with different perpendicular wave numbers $k_{\perp 1}$ and $k_{\perp 2}$ are solutions of the cold plasma dispersion relation. When the two branches are propagating (that is, when the values of $k_{\perp 1,2}$ are real) and are the cause of a sufficiently high rate of energy leakage out of the beam–wave interaction region, one can calculate the beam excited field neglecting the contribution of the parallel electromagnetic energy flux and express the fields through the local value of the slowly varying beam current. On another hand, if one or both branches are evanescent, the energy radiated out of the beam volume can be relatively reduced and, for some ranges of parameters, one should take into account the contribution of the parallel energy flux to the total variation along z of the wave energy. Let us mention that in previous papers the physical features of the nonlinear beam–whistler interaction have been studied as a function of the leakage intensity for the case of a cylindrical beam (parallel beam injection, e.g. [24, 27]), showing how the energy dissipation rate out of the beam essentially modifies the well-known picture of the wave saturation process by particle trapping.

In the present paper, we extend the domain of validity of the theoretical model and the numerical code developed by Volokitin, Krafft and coworkers [22–29] for the case of sheared whistlers radiated by a narrow electron beam in an overdense magnetized plasma; the combined semi-analytical method describing the electromagnetic waves' interaction with the beam in the background plasma is conserved.

This paper is organized as follows. In Sec. 2 we present the nonlinear model and the analytical expressions of the electromagnetic wave fields excited by the narrow spiraling beam in a magnetized cold plasma using Green functions techniques.

https://doi.org/10.1017/S002237780500379X Published online by Cambridge University Press

For completeness, a brief derivation of the formulas is presented in Appendices A, B and C. The linear growth rate of the narrow spiral beam instability is calculated and the corresponding radial power flux is determined. Section 3 is devoted to presenting and to discussing numerical simulation results for different beam–plasma parameters.

2. The nonlinear model

2.1. Electromagnetic wave fields

The original approach developed to study the interaction of a thin spiral electron beam with low-frequency waves has been thoroughly presented in previous papers (e.g. [25]). Thus we only recall here the main features of the related theoretical model and mainly stress the new developments which allow us to extend the range of its applicability. The beam is injected at a finite pitch angle $\beta_{\rm p}$ with respect to the ambient magnetic field $\mathbf{B}_0 = B_0\mathbf{z}$ around which it is spiraling (steady state regime is considered); $\mathbf{z}$ is the unit vector along the parallel direction; all beam electrons are magnetized and assumed not to leave a magnetic tube of radius R. Outside this tube, the waves are propagating free as cylindrical waves out of the beam volume to infinity; inside the tube, the waves' amplitudes are supposed to evolve slowly along $\mathbf{z}$. The beam is assumed to keep its spiral structure due to the Larmor rotation and its initial thickness is typically much less than the spiral radius; however, during its interaction with the waves, the spiral is spread and can evolve to form a hollow cylinder. The waves' fields are determined by the beam current through linear relations depending on the resonance conditions $k_z v_{{\rm b}z} = \omega + m\omega_{\rm c}$ and the dispersion relation in a magnetized infinite background plasma ($\omega_{\rm c} = |eB_0/m_{\rm e}c|$ is the electron gyrofrequency, ω is the wave frequency, m is the resonance number, k_z is the parallel wave number, $v_{{\rm b}z}$ is the parallel beam velocity, $-e < 0$ and $m_{\rm e}$ are the electron charge and mass).

Whereas one specificity of the previous model [25] consisted in the fact that sheared whistler waves were considered and thus that the electromagnetic fields could be derived from the scalar potential and the parallel component of the vector potential only (which allowed some essential simplifications in the analytical calculations), a significative extension of the domain of validity of the model requires to use more classical methods and does not allow one to proceed in such a simplified approach. Indeed, the components of the electromagnetic wave field radiated by a given modulated current of charged particles in a homogeneous background magnetized plasma [51, 52] can be expressed at the position $\mathbf{r}(r, \theta, z)$ as the sum of the partial fields $\mathbf{E}_m^{(j)}$ and $\mathbf{B}_m^{(j)}$ related to the branch j and the resonance number m of the radiated wave

$$\begin{aligned} \mathbf{E}(\mathbf{r}, t) &= \sum_j \sum_m \mathbf{E}_m^{(j)}(r, z) \exp(i\eta) + \text{c.c.}, \\ \mathbf{B}(\mathbf{r}, t) &= \sum_j \sum_m \mathbf{B}_m^{(j)}(r, z) \exp(i\eta) + \text{c.c.}, \end{aligned} \tag{1}$$

where $\eta = k_z z - m\theta - \omega t$ is the phase; r, θ and z are the radial, the azimuthal and the parallel coordinates; $\mathbf{E}_m^{(j)}(E_{rm}^{(j)}, E_{\theta m}^{(j)}, E_{zm}^{(j)})$ and $\mathbf{B}_m^{(j)}(B_{rm}^{(j)}, B_{\theta m}^{(j)}, B_{zm}^{(j)})$ are the Fourier amplitudes of the electric and magnetic fields for the branch j and the harmonic

https://doi.org/10.1017/S002237780500379X Published online by Cambridge University Press

m; c.c. is the complex conjugate. We consider here that the fields amplitudes are slowly varying along the axis $\mathbf{z}$.

Using the integral presentation with Green functions, the slow evolution of the fields' amplitudes $\mathbf{E}_m^{(j)}$ and $\mathbf{B}_m^{(j)}$ along $\mathbf{z}$ during their interaction with the beam can be calculated under some assumptions. Indeed, contrary to the case of the beam injection parallel to $\mathbf{B}_0$ (where a 'cylindrical' beam is considered, e.g. [24]), the model describing the nonlinear evolution of a narrow spiral beam injected at a given pitch angle neglects in the wave energy transport equations—for the numerical calculations only and in order to reduce the computing resources—the variation along $\mathbf{z}$ of the parallel energy flux P_z compared with the radial energy losses [25]. For a narrow beam this simplification does not lead to physical results qualitatively different from those obtained when considering the 'cylindrical' beam case and does not essentially modify the features of the involved physical processes. Under these assumptions the Fourier amplitudes of the electromagnetic fields are given by

$$\begin{pmatrix}\mathbf{E}_m^{(j)}(x)\\ \mathbf{B}_m^{(j)}(x)\end{pmatrix} = i\frac{\pi}{2}\frac{4\pi}{\omega}\frac{g\eta}{\varepsilon}\frac{1}{\sigma_j(S_2^2-S_1^2)}\begin{pmatrix}\mathscr{E}_m^{(j)}(x)\\ \mathscr{B}_m^{(j)}(x)\end{pmatrix}\int_0^\infty \frac{\xi\, d\xi}{S_j^2}\mathscr{P}_m^{(j)}(\xi), \tag{2}$$

where $x = \rho S_j$ and $\rho = r\omega/c$ is the normalized radial coordinate where the field amplitude is calculated; $S_j = ck_{\perp j}/\omega$ is the perpendicular refractive index (for a given parallel refractive index $N_z = ck_z/\omega$); $\xi = (r'\omega/c)S_j$, r' corresponding to the radial position where the current density is localized; ε, g and η are the dielectric permittivity tensor components (see Appendix A) and the parameter $\sigma_j = k_j\alpha_{xj}/k_z$ indicates the sign of the wave polarization sense of the branch j ($k_j^2 = k_{\perp j}^2 + k_z^2$), being negative for electron whistler waves; α_{zj}^0, α_{xj}^0, α_{xj} are the polarization coefficients of the electromagnetic waves in a magnetized plasma [53] (see also (A 10) in Appendix A); $H_m^{(j)}$ is the Hankel function of order m and type j and J_m is the Bessel function of order m [54]. When $\xi \leqslant x$, the functions $\mathscr{P}_m^{(j)}(\xi)$, $\mathscr{E}_m^{(j)}(x)$ and $\mathscr{B}_m^{(j)}(x)$ obtained owing to Green functions techniques are given by (see also Appendix A)

$$\mathscr{P}_m^{(j)}(\xi) = \left[-j_{zm}\alpha_{zj}^0 + \frac{m}{\xi}\left(\alpha_{xj}^0 j_{\theta m} - ij_{\mathrm{r}m}\right)\right]J_m(\xi) + \left(j_{\theta m} - i\alpha_{xj}^0 j_{\mathrm{r}m}\right)J_m'(\xi), \tag{3}$$

$$\mathscr{E}_m^{(j)}(x) = \begin{bmatrix}\dfrac{m}{x}H_m^{(j)}(x) + \alpha_{xj}^0 H_m^{(j)'}(x)\\ -i\alpha_{xj}^0\dfrac{m}{x}H_m^{(j)}(x) - iH_m^{(j)'}(x)\\ i\alpha_{zj}^0 H_m^{(j)}(x)\end{bmatrix},$$

$$\mathscr{B}_m^{(j)}(x) = \begin{bmatrix}iN_z\left[\sigma_j\dfrac{m}{x}H_m^{(j)}(x) + H_m^{(j)'}(x)\right]\\ N_z\left[\dfrac{m}{x}H_m^{(j)}(x) + \sigma_j H_m^{(j)'}(x)\right]\\ S_j H_m^{(j)}(x)\end{bmatrix}, \tag{4}$$

where $j_{\mathrm{r}m}$, $j_{\theta m}$ and j_{zm} are the slowly varying Fourier amplitudes of the current density $\mathbf{j}(j_{\mathrm{r}}, j_\theta, j_z)$ for the harmonic m (below and throughout all the paper we will write $j_{\mathrm{r}m} = j_{\mathrm{r}m}(\xi, z)$, $j_{\theta m} = j_{\theta m}(\xi, z)$ and $j_{zm} = j_{zm}(\xi, z)$); $H_m^{(j)'}$ and J_m' are the derivatives of the Hankel function $H_m^{(j)}$ and the Bessel function J_m. For $\xi \geqslant x$ we

https://doi.org/10.1017/S002237780500379X Published online by Cambridge University Press

have

$$\mathscr{P}_m^{(j)}(\xi)=\left[-j_{zm}\alpha_{zj}^0+\frac{m}{\xi}\left(\alpha_{xj}^0 j_{\theta m}-ij_{\mathrm{r}m}\right)\right]H_m^{(j)}(\xi)+\left(j_{\theta m}-i\alpha_{xj}^0 j_{\mathrm{r}m}\right)H_m^{(j)'}(\xi), \quad (5)$$

$$\mathscr{E}_m^{(j)}(x)=\begin{bmatrix}\dfrac{m}{x}J_m(x)+\alpha_{xj}^0 J_m'(x)\\ -i\alpha_{xj}^0\dfrac{m}{x}J_m(x)-iJ_m'(x)\\ i\alpha_{zj}^0 J_m(x)\end{bmatrix},\quad \mathscr{B}_m^{(j)}(x)=\begin{bmatrix}iN_z\left[\sigma_j\dfrac{m}{x}J_m(x)+J_m'(x)\right]\\ N_z\left[\dfrac{m}{x}J_m(x)+\sigma_j J_m'(x)\right]\\ S_j J_m(x)\end{bmatrix}. \quad (6)$$

Let us remind that the physical meaning of the polarization coefficients can be clarified for a wave field far from the beam axis ($x\to\infty$): in this case $\alpha_{xj}^0=-i\mathscr{E}_{mr}^{(j)}/\mathscr{E}_{m\theta}^{(j)}$ and $\alpha_{zj}^0=i(-1)^j\mathscr{E}_{mz}^{(j)}/\mathscr{E}_{m\theta}^{(j)}$. The fact that the solution (2) corresponds to the case when no energy sources exist far away from the beam imposes that $g\eta\varepsilon\sigma_j(S_2^2-S_1^2)<0$ (see also below (25)); this expression defines the numeration of the roots $k_{\perp j}$ ($j=1,2$) compatible with the kind of Hankel functions used, i.e. $\mathrm{Im}(k_{\perp 1})>0$ and $\mathrm{Im}(k_{\perp 2})<0$ (see also (B 1) in Appendix B). Note that the field expressions (2) present a singularity for $S_2^2=S_1^2$, when the perpendicular group velocity of the both branches vanishes (the narrow beam condition—see the next section—is also no more valid in this case).

Thus, omitting for the coaxial beam case the contribution of the radial current j_{r} (see also [25]), the Fourier amplitudes of the fields at the radial distances $x\lesssim\xi$ are given by

$$\begin{pmatrix}\mathbf{E}_m^{(j)}(x)\\ \mathbf{B}_m^{(j)}(x)\end{pmatrix}=i\frac{\pi}{2}\frac{4\pi}{\omega}\frac{g\eta}{\varepsilon}\frac{1}{\sigma_j(S_2^2-S_1^2)}\begin{pmatrix}\mathscr{E}_m^{(j)}(x)\\ \mathscr{B}_m^{(j)}(x)\end{pmatrix}$$
$$\times\int_0^T\frac{dt}{T}\int_0^{L_z}\frac{k_z dz}{2\pi}\int_0^{2\pi}\frac{d\theta}{2\pi}\int_x^\infty\frac{\xi d\xi}{S_j^2}\left[-H_m^{(j)}(\xi)\alpha_{zj}^0 j_z(t,z,\theta,\xi)\right.$$
$$\left.+\left(H_m^{(j)}(\xi)\frac{m}{\xi}\alpha_{xj}^0+H_m^{(j)'}(\xi)\right)j_\theta(t,z,\theta,\xi)\right]e^{-i\eta}, \quad (7)$$

and for $\xi\lesssim x$ by

$$\begin{pmatrix}\mathbf{E}_m^{(j)}(x)\\ \mathbf{B}_m^{(j)}(x)\end{pmatrix}=i\frac{\pi}{2}\frac{4\pi}{\omega}\frac{g\eta}{\varepsilon}\frac{1}{\sigma_j(S_2^2-S_1^2)}\begin{pmatrix}\mathscr{E}_m^{(j)}(x)\\ \mathscr{B}_m^{(j)}(x)\end{pmatrix}$$
$$\times\int_0^T\frac{dt}{T}\int_0^{L_z}\frac{k_z dz}{2\pi}\int_0^{2\pi}\frac{d\theta}{2\pi}\int_0^x\frac{\xi d\xi}{S_j^2}\left[-J_m(\xi)\alpha_{zj}^0 j_z(t,z,\theta,\xi)\right.$$
$$\left.+\left(J_m(\xi)\frac{m}{\xi}\alpha_{xj}^0+J_m'(\xi)\right)j_\theta(t,z,\theta,\xi)\right]e^{-i\eta}, \quad (8)$$

where L_z is the size of the box used in the numerical simulations ($L_z k_z=2\pi$ when one single wave $\mathbf{k}(\mathbf{k}_\perp,k_z)$ is present); T is the wave period; $\mathbf{j}(t,z,\theta,\xi)$ is the current density. According to the Liouville theorem, (7) and (8) can be expressed through the beam density $n_{\mathrm{b}}(t,z,\theta,\xi)$ as a sum over the N_{p} beam particles distributed inside

https://doi.org/10.1017/S002237780500379X Published online by Cambridge University Press

the box of length L_z and cross-section $S_\perp$

$$\int_0^T \frac{dt}{T}\int_0^{L_z}\frac{k_z\,dz}{2\pi}\int_0^{2\pi}\frac{d\theta}{2\pi}\int_0^{\infty}\xi\,d\xi n_{\rm b}(t,z,\theta,\xi)\exp(-i\eta)$$
$$\to \frac{n_{\rm b}S_\perp}{2\pi}\int_0^T\frac{dt}{T}\frac{1}{N_p}\sum_{p=1}^{N_{\rm p}}\exp(-i\eta_{\rm p}), \tag{9}$$

where $S_\perp$ represents the beam cross-section; the phase $\eta_{\rm p}$ in (9) is calculated at the position of the particle p; $n_{\rm b}$ corresponds to the actual average beam density ($n_{\rm b}S_\perp L_z = N_{\rm p}$). Finally, the Fourier amplitudes of the fields excited by the beam particles at $x \lesssim \xi_{\rm p}$ can be presented, for a given resonance harmonic m, as

$$\begin{pmatrix}\mathbf{E}_m^{(j)}(x)\\ \mathbf{B}_m^{(j)}(x)\end{pmatrix} = -i\pi\frac{g\eta}{\varepsilon}\frac{1}{\sigma_j S_j^2(S_2^2-S_1^2)}\frac{I_{\rm b}}{\omega v_{{\rm b}z}}\begin{pmatrix}\mathscr{E}_m^{(j)}(x)\\ \mathscr{B}_m^{(j)}(x)\end{pmatrix}$$
$$\times\int_0^T\frac{dt}{T}\frac{1}{N_{\rm p}}\sum_{p=1}^{N_{\rm p}}\Big[-H_m^{(j)}(\xi_{\rm p})\alpha_{zj}^0 v_{z{\rm p}}$$
$$+\left(H_m^{(j)}(\xi_{\rm p})\frac{m}{\xi_{\rm p}}\alpha_{xj}^0+H_m^{(j)'}(\xi_{\rm p})\right)v_{\theta{\rm p}}\Big]e^{-i\eta_{\rm p}}, \tag{10}$$

and at $x \gtrsim \xi_{\rm p}$ as

$$\begin{pmatrix}\mathbf{E}_m^{(j)}(x)\\ \mathbf{B}_m^{(j)}(x)\end{pmatrix} = -i\pi\frac{g\eta}{\varepsilon}\frac{1}{\sigma_j S_j^2(S_2^2-S_1^2)}\frac{I_{\rm b}}{\omega v_{{\rm b}z}}\begin{pmatrix}\mathscr{E}_m^{(j)}(x)\\ \mathscr{B}_m^{(j)}(x)\end{pmatrix}$$
$$\times\int_0^T\frac{dt}{T}\frac{1}{N_{\rm p}}\sum_{p=1}^{N_{\rm p}}\Big[-J_m(\xi_{\rm p})\alpha_{zj}^0 v_{z{\rm p}}$$
$$+\left(J_m(\xi_{\rm p})\frac{m}{\xi_{\rm p}}\alpha_{xj}^0+J_m'(\xi_{\rm p})\right)v_{\theta{\rm p}}\Big]e^{-i\eta_{\rm p}}, \tag{11}$$

where $I_{\rm b} = eS_\perp|v_{{\rm b}z}|n_{\rm b}$; $v_{z{\rm p}}$ and $v_{\theta{\rm p}}$ are the parallel and azimuthal velocities of the particle p, respectively.

2.2. Beam particles' motion and narrow beam instability

The time evolution of the beam current is considered self-consistently as the result of the nonlinear beam particles' motion in the fields of the electromagnetic waves (1). For particles which are nearly resonant with this wave (16), an additional simplification can be done in the case when the beam particles follow a quasi-coaxial motion $v(v_z, v_\theta = v_\perp, v_{\rm r} = 0)$ (see also [25]). The variations of the relative particles' phases η and transverse velocities $v_\perp$ are connected through the equations

$$\frac{dv_\perp}{dt} = \frac{d\theta}{dt}\frac{dr}{dt} + r\frac{d^2\theta}{dt^2} \tag{12}$$

$$\frac{d\eta}{dt} = k_z(v_z - v_{{\rm b}z}) - m\left(\frac{d\theta}{dt}-\omega_{\rm c}\right). \tag{13}$$

If $dr/dt \simeq 0$, one can write that

$$\frac{d^2\eta}{dt^2} = k_z\frac{dv_z}{dt} - m\frac{d^2\theta}{dt^2} \simeq k_z\frac{dv_z}{dt} - \frac{m}{r}\frac{dv_\perp}{dt}. \tag{14}$$

https://doi.org/10.1017/S002237780500379X Published online by Cambridge University Press

Using (12) and (14) for a nearly resonant particle p, we have

$$\frac{d^2\eta_{\rm p}}{dt^2} = k_z \frac{dv_{z\rm p}}{dt} - \frac{m\omega_{\rm c}}{v_{\perp\rm p}} \frac{dv_{\perp\rm p}}{dt} \simeq \hat{\tau}_{\rm p}^{-2} \frac{e^{i\eta_{\rm p}}}{2} + \text{c.c.}, \tag{15}$$

where $\hat{\tau}_{\rm p}$ is the characteristic time scale of the resonant particles' oscillations; if the small terms corresponding to the scattering of the particles' velocities near $v_{{\rm b}z}$ are neglected

$$\frac{m\omega_{\rm c}}{k_z v_{\perp\rm p}} \left| \frac{v_{z\rm p} - v_{{\rm b}z}}{v_{\perp\rm p}} \right| \ll \left\{ 1, \frac{m^2\omega_{\rm c}^2}{k_z^2 v_{\perp\rm p}^2} \right\}, \tag{16}$$

then the expression for $\hat{\tau}_{\rm p}$ can be written as

$$\hat{\tau}_{\rm p}^{-2} \simeq \left| \left(1 + \frac{m^2\omega_{\rm c}^2}{v_{\perp\rm p}^2} \right) k_z \omega_{\rm c} \sum_{j=1}^{2} h_j W_j(x_{j\rm p}) \right|, \tag{17}$$

where h_j and $W_j(x_{j\rm p})$ are defined in Appendix C.

The influence of the phase evolution of all the particles on the resultant wave fields' variations (i.e. on the values of the growth rate γ and the frequency shift $\delta\omega$ for fields' amplitudes $\propto \exp(\gamma t - i\delta\omega t)$) can be estimated analytically for the case of a narrow beam, following the scheme of Volokitin and Krafft [25]. Actually, at the initial stage of the evolution, one can solve (15) in the so-called linear approximation by substituting in its right-hand side the particles' phase evolution in the undisturbed approximation, i.e. $\eta_{\rm p} - \eta_{0\rm p} \simeq k_z(v_{z\rm p} - v_{{\rm b}z})t$,

$$\begin{aligned} &\delta\eta_{\rm p} \left(1 - \left[\frac{i}{2} \frac{\hat{\tau}_0^{-2} e^{i\eta_{\rm p}}}{[ik_z(v_{z\rm p} - v_{{\rm b}z}) + \gamma - i\delta\omega]^2} + \text{c.c.} \right] \right) \\ &\quad \simeq \frac{\hat{\tau}^{-2} - \hat{\tau}_0^{-2}}{[ik_z(v_{z\rm p} - v_{{\rm b}z}) + \gamma - i\delta\omega]^2} \frac{e^{i\eta_{\rm p}}}{2} + \text{c.c.}, \end{aligned} \tag{18}$$

where $\delta\eta_{\rm p} \equiv \eta_{\rm p} - \eta_{0\rm p}$ and $\hat{\tau} - \hat{\tau}_0$ are the variations of the phase of the particle p and the oscillation time. The variation of $\hat{\tau}^{-2}$ due to the field variation resulting from the phase variation $\delta\eta_{\rm p}$ (at the initial stage, the particles of the thin beam have approximately the same radial position which corresponds to the beam Larmor radius $r_{\rm L}$; that is, $\hat{\tau}_{\rm p} = \hat{\tau}$ for each resonant particle (17)) is given by

$$\hat{\tau}^{-2} - \hat{\tau}_0^{-2} = \hat{\tau}_0^{-2}(\exp(\gamma - i\delta\omega)t - 1) = \Theta \int_0^T \frac{dt}{T} \frac{1}{N_{\rm p}} \sum_{p=1}^{N_{\rm p}} e^{-i\eta_{\rm p}}(-i)\delta\eta_{\rm p} \tag{19}$$

where

$$\begin{aligned} \Theta = &\left(1 + \frac{m^2\omega_{\rm c}^2}{v_\perp^2} \right) \frac{\omega^2}{c^2} \left(\frac{g\eta}{\varepsilon} \right) \left| \frac{k_z^3 c^3}{\omega^3} \right| \frac{\omega}{|k_z v_{{\rm b}z}|} \left| \frac{2\pi I_{\rm b} e}{m_{\rm e} c^3} \right| \frac{1}{(S_2^2 - S_1^2)} \\ &\times \sum_{j=1}^{2} \frac{1}{\sigma_j} W_j^{\rm H}(k_{\perp j} r_{\rm L}) W_j^{\rm B}(k_{\perp j} r_{\rm L}), \end{aligned} \tag{20}$$

and (see (C 6) in Appendix C)

$$\begin{aligned} W_j^{\rm B}(x_j) &= c \frac{\sigma_j}{\eta} \frac{N_j^2}{S_j} \left\{ \frac{S_j^2}{N_j^2} J_m(x_j) + \frac{\eta}{N_j^2} \frac{\omega_{\rm c}}{\omega} x_j \left[\frac{m}{x_j} J_m(x_j) + \frac{1}{\sigma_j} J'_m(x_j) \right] \right\}, \\ W_j^{\rm H}(x_j) &= c \frac{\sigma_j}{\eta} \frac{N_j^2}{S_j} \left\{ \frac{S_j^2}{N_j^2} H_m^{(j)}(x_j) + \frac{\eta}{N_j^2} \frac{\omega_{\rm c}}{\omega} x_j \left[\frac{m}{x_j} H_m^{(j)}(x_j) + \frac{1}{\sigma_j} H_m^{(j)'}(x_j) \right] \right\}. \end{aligned} \tag{21}$$

https://doi.org/10.1017/S002237780500379X Published online by Cambridge University Press

Supposing that initially the beam particles are distributed uniformly over the phases, one has

$$\hat{\tau}_0^{-2} = \Theta \int_0^T \frac{dt}{T} \frac{1}{N_\mathrm{p}} \sum_{p=1}^{N_\mathrm{p}} e^{-i\eta_{0\mathrm{p}}} \simeq 0. \tag{22}$$

Multiplying the left-hand side of (18) by $\exp(-i\eta_\mathrm{p})$ and performing the summation over all the beam particles inside the simulation box, one gets

$$1 \simeq -\frac{1}{N_\mathrm{p}} \sum_{p=1}^{N_\mathrm{p}} \frac{1}{[ik_z(v_{z\mathrm{p}} - v_{\mathrm{b}z}) + \gamma - i\delta\omega]^2} \frac{i\Theta}{2}. \tag{23}$$

If the beam is quasi-monoenergetic, $k_z^2(v_{z\mathrm{p}} - v_{\mathrm{b}z})^2 \ll \gamma^2 + \delta\omega^2$, one obtains

$$(\gamma - i\delta\omega)^2 \simeq -\frac{i\Theta}{2} \propto \frac{n_\mathrm{b}}{n_\mathrm{p}}, \quad \gamma \simeq \mathrm{Re}\left[\sqrt{-\frac{i\Theta}{2}}\right], \tag{24}$$

where n_p is the background plasma density. One can see that the linear growth rate calculated taking into account the narrow beam conditions is proportional to $(n_\mathrm{b}/n_\mathrm{p})^{1/2}$ while in the wide beam case one has $\gamma \propto (n_\mathrm{b}/n_\mathrm{p})^{1/3}$ [20].

One of the most important physical parameters governing the evolution of the system is the beam size perpendicular to the magnetic field. The beam can be considered as narrow when the electromagnetic energy leakage in the perpendicular direction exceeds the accumulation rate of energy inside the interaction region. This condition can be written in a draft manner as $\gamma r_\mathrm{L} < v_{\mathrm{g}\perp}$ [20], where $v_{\mathrm{g}\perp}$ is the perpendicular group velocity of the propagating whistler branch. The simulation code developed by Volokitin and Krafft [25] is applicable in this case and the field components governing the particles' motion can be calculated using Green functions techniques for a given modulated current slowly varying along the ambient magnetic field. Calculating for each branch j the term

$$\frac{(\mathbf{k}_\perp \cdot \mathbf{v}_{\mathrm{g}\perp})_j}{\omega} = 2S_j^2 \frac{\varepsilon}{g\eta} \frac{\alpha_{xj}}{\cos\phi_j} \frac{(S_j^2 - S_{\neq j}^2)}{(1+\alpha_{xj}^2)} \left[\frac{\partial}{\omega\partial\omega}\omega^2 \,\mathrm{Re}\, N_j^2(\omega,\phi_j)\right]^{-1}, \tag{25}$$

where $N_j(\omega,\phi_j)$ is the refractive index expressed as a function of the frequency and the angle ϕ_j between $\mathbf{k}_j$ and $\mathbf{B}_0$, one can obtain the domain of validity of the narrow beam condition as well as the dependence of γ on r_L, i.e. on the pitch angle.

2.3. Radial electromagnetic power flux

The radial electromagnetic power flux per unit length of the beam, $2\pi r P_\mathrm{r}$, can be calculated using expressions (A 15) and (A 19)–(A 22) outside the beam region. In the case when the two whistler branches are propagating (i.e. they contribute both to the field excited outside of the beam), one can expect that the resultant field will produce an interference pattern so that the radial energy flux will reveal spatial oscillations. However, the actual time averaged value of the radial component of the Poynting vector outside of the beam region does not contain any spatially oscillating terms; each branch contributes to the radial power flux independently. This feature originates from the fact that the fields of both branches are resonantly excited by the same current (they have the same parallel refractive index) and that the field polarization coefficients of both branches are linked through the dispersion relation [53].

https://doi.org/10.1017/S002237780500379X Published online by Cambridge University Press

The radial component of the electromagnetic power averaged over the time can be expressed as follows (the numeration of the roots provides the inequality $\sigma_j(S_2^2 - S_1^2)\varepsilon\eta/g < 0$ (B 1))

$$P_{\rm r} = \frac{c}{4\pi}[E_\theta B_z^* - E_z B_\theta^* + \text{c.c.}] = \sum_{j=1,2} P_{{\rm r}j} = -\frac{(S_2^2 - S_1^2)}{\pi^2 r\omega}\frac{\varepsilon\eta}{g}\frac{\omega^2}{k_z^2}\sum_{j=1,2}\frac{1}{\sigma_j}\frac{|\Psi_j|^2}{S_j^2}, \quad (26)$$

with

$$\Psi_j = \pi\frac{\omega}{c^2}\left|\frac{I_{\rm b}}{ev_{{\rm b}z}}\right|\frac{g}{\varepsilon}\frac{S_j N_z}{(S_2^2 - S_1^2)}\langle W_j^{\rm B}\rangle, \quad E_{zm}^{(j)}(x_j) = \Psi_j H_m^{(j)}(x_j), \quad (27)$$

and (see also (21))

$$\langle W_j^{\rm B}\rangle \equiv \int_0^T \frac{dt}{T}\frac{1}{N_{\rm p}}\sum_{p=1}^{N_{\rm p}} W_j^{\rm B} e^{-i\eta_{\rm p}}. \quad (28)$$

For a propagating branch, when $\text{Im}(S_j^2) = 0$, one has $P_{{\rm r}j} > 0$; in contrast, an evanescent branch does not contribute to the radial power flux and $P_{{\rm r}j} = 0$.

3. Numerical simulations

The equations for the wave fields' evolution (10)–(11) and the particles' motion (with full nonlinearities included) have been solved numerically for various physical parameters and for different resonance conditions $k_z v_{{\rm b}z} = \omega + m\omega_{\rm c}$ ($m = 0, -1, 1$; that is, Landau, normal and anomalous cyclotron resonances, respectively). A leap-frog method was used to push the $N_{\rm p}$ macro-particles ($2000 \lesssim N_{\rm p} \lesssim 10\,000$) moving in the electromagnetic fields; those are calculated on fixed mesh grids and interpolated using bicubic splines on the particles' positions inside the beam tube. Since in our model no fast time variation of the wave fields is taken into account, the high-frequency physical oscillations of their phases and amplitudes have been suppressed when necessary by an adequate averaging over one or several cyclotron periods. Initially, the total beam current is slightly modulated along the longitudinal direction z and the electrons are distributed on a spiral with small perpendicular velocities' and positions' spreading, of the order of 10% typically.

Note that in this section, all variables (even when already used previously with the same name) refer to normalized values.

3.1. Landau resonance

Figure 1(a) shows for the case of the Landau resonance ($k_z v_{{\rm b}z} = \omega$) the variation of the normalized growth rate γ/ω (24) as a function of the beam injection pitch angle $\beta_{\rm p}$. Note that k_z varies with $\beta_{\rm p}$ as the beam energy $E_{\rm b}$ fixed. The behavior of γ/ω is non-monotonic, due to the wave structure imposed by the Green functions and the resultant expression for the nonlinear evolution time $\hat{\tau}$ (17). Figure 1(b) presents the variation of the radial power flux $2\pi r P_{\rm r}$ per unit beam length in W m^{-1} (26) as a function of $\beta_{\rm p}$, for a fixed beam current $I_{\rm b}$. One can see that for the chosen parameters, the whistler dispersion relation does not have—for a fixed k_z—a real solution $k_\perp$ if $\beta_{\rm p} \lesssim 27^\circ$ (in this case, both waves are evanescent and cannot propagate outside the beam). The whistler dispersion relation is shown in Fig. 2 in the form of an index surface $(ck_\perp/\omega, ck_z/\omega)$ ($\omega_{\rm p}/\omega_{\rm c}$ and $\omega/\omega_{\rm c}$ are fixed); the resonance condition is indicated by the horizontal line $ck_z/\omega = c/v_{{\rm b}z}$ (Landau resonance), pointing out the two propagating whistler branches $(k_{\perp 1}, k_z)$ and $(k_{\perp 2}, k_z)$ for $\beta_{\rm p} = 50^\circ$, that is, $ck_z/\omega = 3.8$.

https://doi.org/10.1017/S002237780500379X Published online by Cambridge University Press

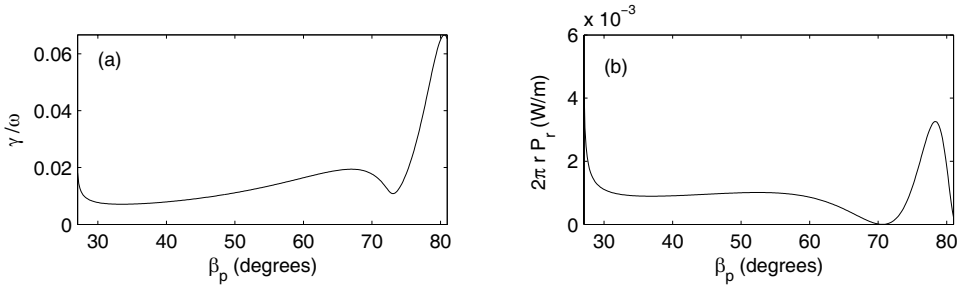


Figure 1. Variation as a function of the injection pitch angle $\beta_{\rm p}$ (in degrees) of (a) the normalized whistler growth rate γ/ω and (b) the radial power flux per unit beam length, $2\pi r P_{\rm r}$ (in W m^{-1}). The main parameters are the following: $E_{\rm b} = 43$ keV, $I_{\rm b} = 0.1$ A, $\omega/\omega_c = 0.05$, $\omega_{\rm p}/\omega_{\rm c} = 1.25$, $m = 0$ (Landau resonance).

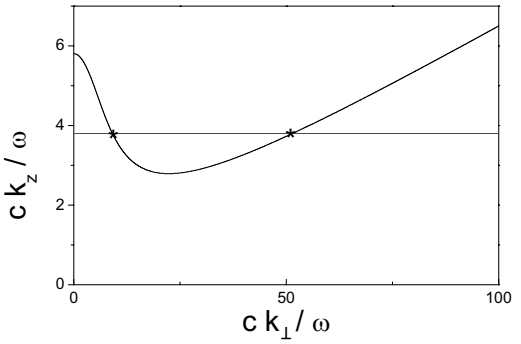


Figure 2. Whistler index surface: variation of the normalized value of the parallel wave number ck_z/ω as a function of the normalized value of the perpendicular wave number $ck_\perp/\omega$. The main parameters are the same as in Fig. 1; the horizontal line corresponds to $\beta_{\rm p} = 50^\circ$ (Landau resonance).

Numerical simulations have been performed for two different values of $\beta_{\rm p}$, keeping the total beam energy and current as well as the background plasma ratio $\omega_{\rm p}/\omega_{\rm c}$ and the normalized wave frequency $\omega/\omega_{\rm c}$ fixed. Figure 3(a) shows for $\beta_{\rm p} = 50^\circ$ the variation of the normalized radial flux $P_{\rm w}$ of wave energy density per unit beam length as a function of the normalized time $\tau = \omega_{\rm c} t/2\pi$; $P_{\rm w}$ is qualitatively very similar to the variation of the normalized wave energy density integrated over the total beam cross-section. Note that the normalized time τ is proportional to the distance Z from the beam injector, $\tau = \omega_{\rm c} Z/2\pi v_{{\rm b}z}$. After linear wave amplitude growth and saturation (Fig. 3(a)), $P_{\rm w}$ shows oscillations around a decreasing mean level which accompany the beam deceleration along the parallel direction during all the evolution time. This can be observed in Fig. 3(b) which presents the variation of the average normalized perpendicular energy change $\Delta E_\perp = \sum_{i=1}^{N_{\rm p}} (v_{\perp i}^2 - v_{\perp 0}^2)/N_{\rm p} = 0$ and of the total beam energy change $\Delta E = \Delta E_\perp + 2p_z = 2p_z$ ($p_z \propto \langle v_z \rangle = \sum_{i=1}^{N_{\rm p}} v_{z{\rm i}}/N_{\rm p}$ is the total normalized parallel momentum). No noticeable evolution can be observed in the perpendicular particles' motion. The beam loses its energy ($\Delta E < 0$) which is continuously transferred to the wave that gradually damps, due to the electromagnetic energy dissipation out of the bounded beam volume. The formed electron bunch, which results from the 'partial' trapping of the electrons

https://doi.org/10.1017/S002237780500379X Published online by Cambridge University Press

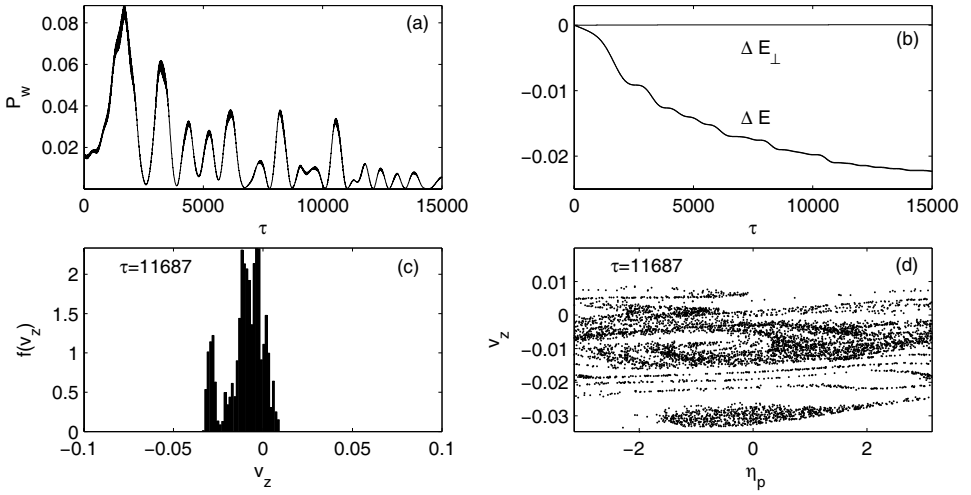


Figure 3. Beam–wave interaction at the Landau resonance ($\omega = k_z v_{bz}$): (a) variation as a function of the normalized time $\tau = \omega_c t/2\pi$ of the normalized radial flux of wave energy P_w per unit beam length; (b) variation as a function of τ of the perpendicular beam energy change $\Delta E_\perp \simeq 0$ and the total beam energy change $\Delta E < 0$ (beam energy loss); (c) distribution $f(v_z)$ of the normalized parallel velocity v_z (in the beam frame, that is, in the frame moving with the initial parallel beam velocity v_{bz}) at $\tau = 11\,687$; (d) phase space at $\tau = 11\,687$ representing the normalized parallel velocity v_z (in the beam frame) as a function of the phase η_p. The main parameters are the following: $\omega_p/\omega_c = 1.25, \omega/\omega_c = 0.05, \beta_p = 50°$, $m = 0$, $N_p = 6000$.

resonantly interacting with the wave [23, 27], is continuously decelerated along z whereas the bulk of the non-resonant particles is heated and exhibits vortices in formation (see Fig. 3(d), for $\tau = 11\,687$). The velocity distribution function $f(v_z)$ of the beam particles is presented for the same time as in Fig. 3(c). Note that the parallel velocity v_z is expressed in the beam frame; that is, in the frame moving with the initial parallel beam velocity v_{bz}.

For another pitch angle value, $\beta_p = 65°$, the evolution of P_w as a function of τ (Fig. 4(a)) is quantitatively different from that shown in Fig. 3(a). Here the wave saturates at a higher amplitude level and presents oscillations around a mean level that decreases very slowly with the time; indeed, in this case, the decelerated bunch (Fig. 4(d)) contains a very large proportion of the total number of particles and thus it is able to support the wave at a significant amplitude and over a long time, although some wave energy is continuously dissipated outside the beam volume (the wave damping stage is not shown here). The decelerated bunch can also be clearly seen in Fig. 4(c) where the bulk of non-resonant particles exhibits a complex structure containing vortices in formation (see also Fig. 4(d)).

3.2. Cyclotron resonances

Figures 5(a) and (b) show the variations of the normalized growth rate γ/ω and of the radial power flux $2\pi r P_r$ per unit beam length as a function of the beam injection pitch angle β_p, in the case when two propagating whistler branches resonantly interact with the beam at the normal cyclotron resonance ($k_z v_{bz} = \omega - \omega_c$). As for the Landau resonance case, one can see that for fixed beam energy, beam current and background plasma, the pitch angle value plays an important role in the efficiency

https://doi.org/10.1017/S002237780500379X Published online by Cambridge University Press

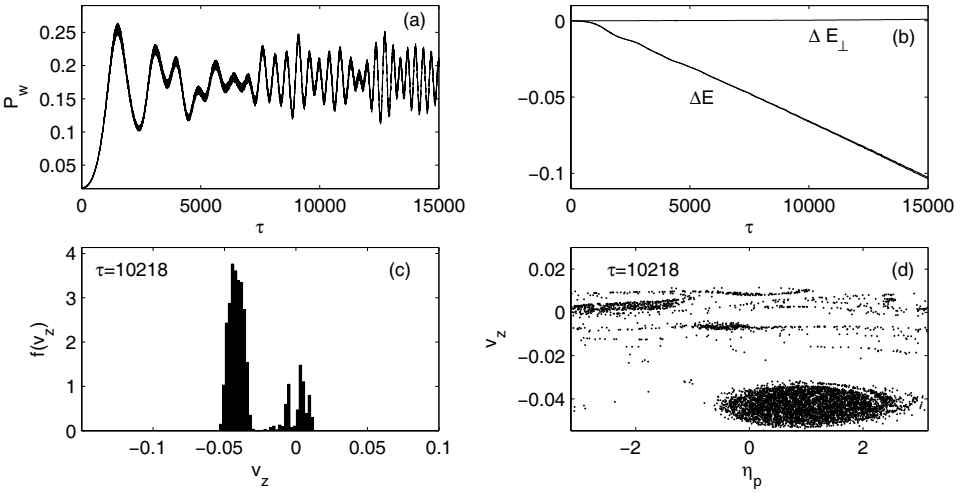


Figure 4. Beam–wave interaction at the Landau resonance ($\omega = k_z v_{bz}$): (a) variation as a function of τ of the normalized radial flux of wave energy P_w per unit beam length; (b) variation as a function of τ of the perpendicular beam energy change $\Delta E_\perp \simeq 0$ and the total beam energy change $\Delta E < 0$ (beam energy loss); (c) distribution $f(v_z)$ of the normalized parallel velocity v_z (in the beam frame) at $\tau = 10\,218$; (d) phase space at $\tau = 10\,218$ representing the normalized parallel velocity v_z (in the beam frame) as a function of the phase η_p. The main parameters are the following: $\omega_p/\omega_c = 1.25$, $\omega/\omega_c = 0.05$, $\beta_p = 65°$, $m = 0$, $N_p = 6000$.

of the beam emission. Indeed, the specific dependencies of γ/ω and $2\pi r P_r$ on β_p, due to the structure of the fields radiated by the spiralling beam, lead to the fact that, in actual space experiments involving beam injection by a gun located on a rotating satellite, one should expect that the beam emission, even if the beam injection angle is fixed, will reveal a nonmonotonic behavior with fields' amplitudes maxima and minima depending on the time of registration. The sharp features in Figs 5(a) and (b) correspond to the case when the first whistler branch becomes evanescent at the point where the real value of its perpendicular wave number vanishes.

Figure 5(c) shows the variation of P_w as a function of τ: the linear growth of the wave amplitude is followed by saturation and slow damping. For the cyclotron resonances, the main energy exchanges during the nonlinear beam-wave evolution occur between the perpendicular and the parallel particles' motions: only a part of the energy, proportional to ω/ω_c, is transferred to the wave, as one can see in Fig. 5(d) which presents the variation as a function of τ of the total normalized parallel momentum p_z, the total beam energy change ΔE and the average normalized perpendicular energy change $\Delta E_\perp$. The growth of p_z is related to the formation of an accelerated electron bunch, as shown by the phase space $\eta_p - v_z$ at $\tau = 213$ (Fig. 5(f)) and by the shape of the parallel velocity distribution function (see $f(v_z)$ in Fig. 5(e)). The increase of p_z is mainly due to particles which strongly interact with the wave; the decreasing perpendicular energy, due to resonant electron focusing and beam perpendicular cooling, provides energy for bunch acceleration.

The last example concerns the beam-wave interaction at the anomalous cyclotron resonance ($k_z v_{bz} = \omega + \omega_c$). The variations of γ/ω and $2\pi r P_r$ as a function of β_p are presented in Figs 6(a) and (b) for the case when the two whistler branches are propagating. Similar conclusions as stated above can be done. Figures 6(c) and

https://doi.org/10.1017/S002237780500379X Published online by Cambridge University Press

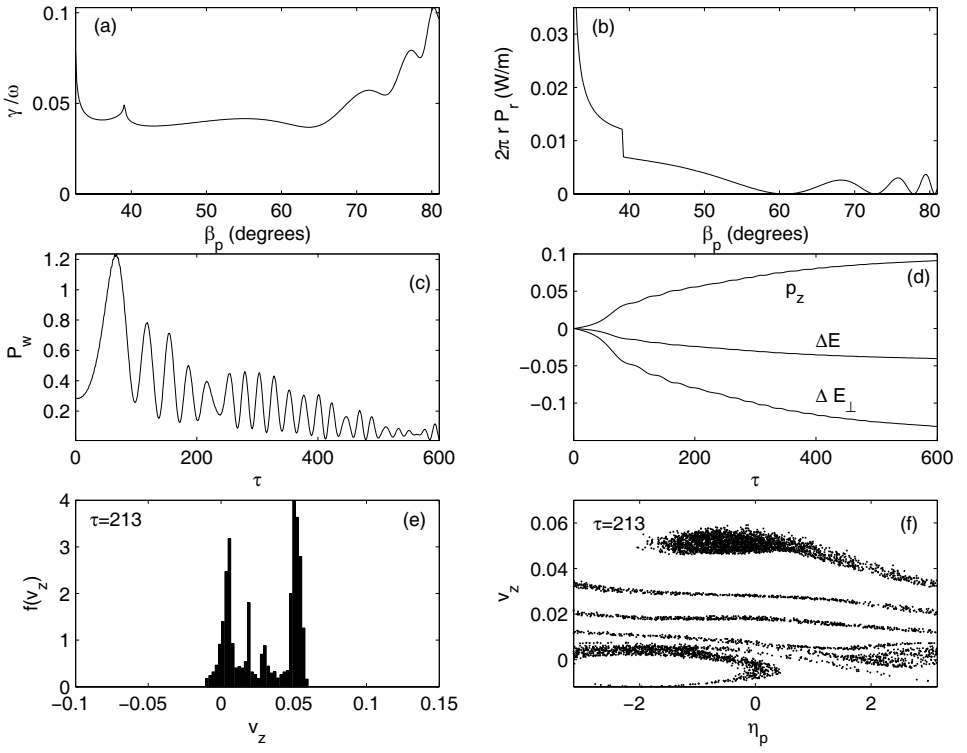


Figure 5. Beam–wave interaction at the normal cyclotron resonance ($\omega - \omega_c = k_z v_{bz}$): variation as a function of the injection pitch angle β_p (in degrees) of (a) the normalized whistler growth rate γ/ω and (b) the radial power flux per beam length, $2\pi r P_r$ (in W m^{-1}); (c) variation as a function of τ of the normalized radial flux of wave energy P_w per unit beam length; (d) variation as a function of τ of the perpendicular beam energy change $\Delta E_\perp < 0$, the total beam energy change $\Delta E < 0$ (beam energy loss) and the average parallel momentum $p_z > 0$; (e) distribution $f(v_z)$ of the normalized parallel velocity v_z (in the beam frame) at $\tau = 213$; (f) phase space at $\tau = 213$ representing the normalized parallel velocity v_z (in the beam frame) as a function of the phase η_p. The main parameters are the following: $\omega_p/\omega_c = 5$, $\omega/\omega_c = 0.3$, $\beta_p = 36°$, $m = -1$, $N_p = 6000$.

(f) show that the energy lost by the beam ($\Delta E < 0$ on the Fig. 6(d)) during its deceleration is transferred for a small part to heat the non-resonant bulk in the parallel direction (Figs 6(e) and (f)) as well as to excite and to sustain the wave emitting electromagnetic radiation outside the beam volume (Fig. 6(c)), and, for the major part, to perpendicular heating ($\Delta E_\perp > 0$ in the Fig. 6(d)). The particles interacting strongly with the wave are gathered in the decelerating bunch, as shown in Figs 6(e) and (f).

3.3. Discussion

The results of the numerical simulations performed for various beam-plasma parameters have revealed that the general features characterizing the nonlinear evolution of a radially bounded beam interacting with an electromagnetic wave are qualitatively the same as found in previous investigations for the limiting case of sheared whistlers in an overdense plasma [24, 25]. The main physical process occurring during the dissipative beam–wave interaction—that is, which takes into

https://doi.org/10.1017/S002237780500379X Published online by Cambridge University Press

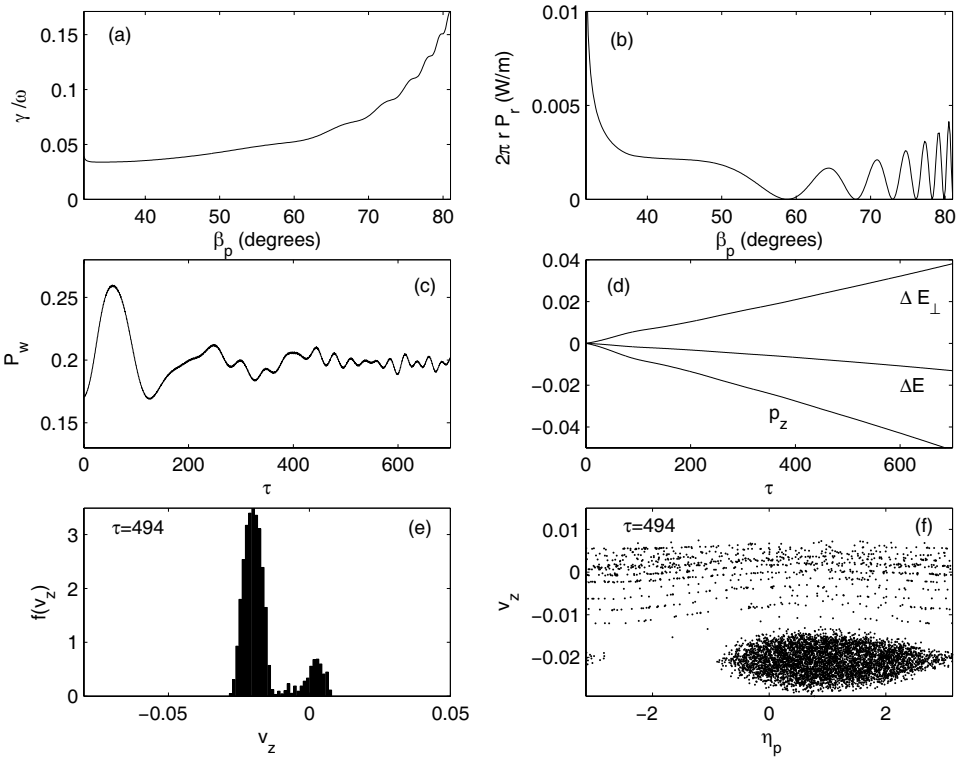


Figure 6. Beam–wave interaction at the anomalous cyclotron resonance ($\omega + \omega_c = k_z v_{bz}$): variation as a function of the injection pitch angle β_p (in degrees) of (a) the normalized whistler growth rate γ/ω and (b) the radial power flux per unit beam length, $2\pi r P_r$ (in W m^{-1}); (c) variation as a function of τ of the normalized radial flux of wave energy P_w per unit beam length; (d) variation as a function of τ of the perpendicular beam energy change $\Delta E_\perp > 0$, the total beam energy change $\Delta E < 0$ (beam energy loss) and the average parallel momentum $p_z < 0$; (e) distribution $f(v_z)$ of the normalized parallel velocity v_z (in the beam frame) at $\tau = 494$; (f) phase space at $\tau = 494$ representing the normalized parallel velocity v_z (in the beam frame) as a function of the phase η_p. The main parameters are the following: $\omega_p/\omega_c = 5$, $\omega/\omega_c = 0.3$, $\beta_p = 36°$, $m = 1$, $N_p = 6000$.

account the energy leakage out of the bounded beam volume—is the nonlinear self-organization of part of the beam electrons which leads to the formation of dynamically stable and longtime living bunches that are continuously decelerated or accelerated while keeping resonance with the emitted wave. In a long time evolution, the bunch(es) is(are) the main cause which support(s) the wave emission whereas the non-resonant beam electrons exchange no energy with the wave.

Let us however discuss some points which can affect the validity of the model for some ranges of parameters. Indeed, the transverse energy leakage, responsible for the bunches' formation, vanishes when both the whistler branches are evanescent (that is, when the real and the imaginary parts of their perpendicular wave numbers are different from zero), what corresponds to the condition $N_z < \min\{N_G, N_P\}$ for any frequency, with

$$N_G^2 = \chi \left\{ 2\left(1 - \frac{\eta}{\chi}\right)\cos^2\alpha_R \left[1 + \sqrt{\left(\frac{\eta}{\chi} + \tan^2\alpha_R\right) \Big/ \left(\frac{\eta}{\chi} - 1\right)} \right] - 1 \right\},$$

https://doi.org/10.1017/S002237780500379X Published online by Cambridge University Press

$$\chi = \varepsilon - g^2/(\varepsilon - \eta), \quad \cos^2 \alpha_{\mathrm{R}} = \varepsilon/(\varepsilon - \eta), \tag{29}$$

$$N_{\mathrm{P}}^2 = \varepsilon - g. \tag{30}$$

At $N_z = N_{\mathrm{G}}$ (respectively, at $N_z = N_{\mathrm{P}}$) the perpendicular group velocity (respectively, the perpendicular wave number) vanishes. When the two waves are evanescent, even for a rather thin beam the absence of transverse energy leakage out of the beam volume can lead to an efficient interaction between the particles and the whistler wave field confined inside the beam tube; then the narrow beam model is no more valid and one should include in the analytical developments the influence of the parallel electromagnetic energy flux gradient on the resultant wave field evolution along the beam tube, which should be independent of the relative leakage rate out of the interaction region. This problem will be the subject of a forthcoming paper. Actually, the influence of the evanescent wave fields is hidden for a remote observer as only the propagating part of the field can transport energy out of the beam region; however, the level of the resultant beam emissivity should be influenced by the evanescent wave excitation. Let us mention that evanescent wave fields can be registered in the near surrounding of an electron beam injected in space [14] as well as in laboratory plasma experiments evidencing field excitation in non-transparent frequency domains [39,56] (in a cold dense plasma, between the electron cyclotron and plasma frequencies and near the electron gyroharmonics).

The case when the second branch (quasi-resonant branch $j = 2$ or Trievelpiece–Gould mode) is propagating and the first branch (electromagnetic branch $j = 1$ or helicon mode) is purely evanescent (i.e. when $S_1^2 < 0$, $\mathrm{Im}(S_1^2) = 0$), is realized for any frequency and $N_z > N_{\mathrm{P}}$. Then, for some ranges of parameters, the propagating branch can provide a sufficiently high rate of energy density leakage so that the total wave field energy density accumulated inside the beam volume will be comparatively small and will not prevent the occurrence of the nonlinear processes described above, as has been shown by numerical simulations (note that the equations for both whistler branches are linked to each other, at least, via their common resonant particles). Finally, the condition for both whistler branches to propagate is $N_{\mathrm{G}} < N_z < N_{\mathrm{P}}$: various examples relative to this case have been presented in this paper.

Acknowledgements

The authors acknowledge the Centre National de la Recherche Scientifique (CNRS, France, PICS 1310), the Institut Universitaire de France (Paris) and the Russian Academy of Sciences for their financial support; this work was also partially supported by the RFBR Grant 03-05-64553a.

Appendix A. Electromagnetic field solutions using Green functions

After the Fourier transformations over the time t and the parallel coordinate z, the set of the Maxwell equations with external current sources can be reduced to a system of two second-order differential equations (for the case without current source terms, see, for example, [57])

$$\nabla_\perp^2 \begin{pmatrix} \bar{E}_z \\ \bar{B}_z \end{pmatrix} + \begin{pmatrix} A & B \\ D & C \end{pmatrix} \begin{pmatrix} \bar{E}_z \\ \bar{B}_z \end{pmatrix} = \begin{pmatrix} Q_1 \\ Q_2 \end{pmatrix}, \tag{A 1}$$

https://doi.org/10.1017/S002237780500379X Published online by Cambridge University Press

where $\bar{E}_z(\omega, k_z)$ and $\bar{B}_z(\omega, k_z)$ correspond to the Fourier amplitudes of the parallel electromagnetic fields; $\nabla_\perp^2$ is the perpendicular dimensionless Laplacian operator (we recall that all of the space variables are normalized to c/ω) and

$$A = \eta\left(1 - \frac{N_z^2}{\varepsilon}\right), \quad B = -iN_z\frac{g}{\varepsilon}, \quad D = -\eta B, \quad C = \varepsilon - N_z^2 - \frac{g^2}{\varepsilon}, \tag{A 2}$$

where $N_z = ck_z/\omega$; ε, g and η are the components of the cold plasma dielectric permittivity tensor [53]

$$\hat{\varepsilon} = \begin{pmatrix} \varepsilon & ig & 0 \\ -ig & \varepsilon & 0 \\ 0 & 0 & \eta \end{pmatrix}. \tag{A 3}$$

The terms representing the external source currents in an homogeneous cold background plasma are given by

$$Q_1 = \frac{4\pi}{\omega} i\left(\frac{N_z}{\varepsilon} c\bar{\rho}_q - \bar{j}_z\right), \quad Q_2 = \frac{4\pi}{\omega}\left(\frac{g}{\varepsilon} c\bar{\rho}_q - [\nabla \times \bar{\mathbf{j}}]_z\right), \tag{A 4}$$

where $\bar{\mathbf{j}}(\bar{\mathbf{j}}_\perp, \bar{j}_z)$ and $\bar{\rho}_q$ are the Fourier amplitudes of the current density and the charge density, so that the continuity equation for the external current has the form

$$ic\bar{\rho}_q = \nabla \cdot \bar{\mathbf{j}}_\perp + iN_z\bar{j}_z. \tag{A 5}$$

The solution of the system (A 1) can be found in the form

$$\begin{pmatrix} \bar{E}_z \\ \bar{B}_z \end{pmatrix} = \bar{E}_z^{(1)}\begin{pmatrix} 1 \\ b_1 \end{pmatrix} + \bar{E}_z^{(2)}\begin{pmatrix} 1 \\ b_2 \end{pmatrix}, \tag{A 6}$$

where the values $b_1 \neq b_2$ depend on k_z and ω, but not on the coordinates

$$b_j = \left(S_j^2 - A\right)/B. \tag{A 7}$$

S_j^2 are the eigenvalues of the matrix in (A 1), corresponding to the eigenvectors $(1, b_j)$

$$A + Bb_j = S_j^2, \quad D + Cb_j = S_j^2 b_j. \tag{A 8}$$

Actually $j = 1, 2$ in (A 8) numerates the two different solutions of the dispersion equation for the perpendicular refractive index $S_j = ck_{\perp j}/\omega$, when the parallel refractive index $N_z = ck_z/\omega$ and the frequency ω are fixed. One has to pay attention that for the evanescent branches, S_j^2 can be negative or complex, even in a plasma without losses, i.e. when ε, g, η, and N_z have real values.

As a representative example, the differential equation for $\bar{E}_z^{(1)}$ can be written as (for $\bar{E}_z^{(2)}$, all the subscripts $j = 1$ should be modified to $j = 2$)

$$(b_1 - b_2)\left(\nabla_\perp^2\bar{E}_z^{(1)} + S_1^2\bar{E}_z^{(1)}\right) = Q_2 - b_2 Q_1 = \frac{4\pi}{\omega}\left\{-\bar{j}_z\alpha_{z1}^0 S_1 - [\nabla \times \bar{\mathbf{j}}]_z + i\alpha_{x1}^0 \nabla \cdot \bar{\mathbf{j}}_\perp\right\}, \tag{A 9}$$

where the polarization coefficients α_{xj}, α_{xj}^0 and α_{zj}^0 correspond to those calculated for plane waves [53] and can be expressed through b_j as

$$\alpha_{xj}^0 = -g\frac{S_j^2 - \eta}{\varepsilon B b_j}, \quad \alpha_{zj}^0 = -g\frac{N_z S_j}{\varepsilon B b_j} = \frac{S_j}{ib_j}, \quad N_j\alpha_{xj} = g\frac{N_z\eta}{\varepsilon B b_j} = -\alpha_{zj}^0\frac{\eta}{S_j}, \tag{A 10}$$

where $N_j = ck_j/\omega$. In the case of a Fourier harmonic of the form $\exp(-im\theta - i\omega t + ik_z z)$, (A 9) reduces itself to the Bessel equation and can be solved in a

https://doi.org/10.1017/S002237780500379X Published online by Cambridge University Press

straightforward manner

$$\frac{1}{x}S_1^2(b_1-b_2)\left[\frac{\partial}{\partial x}\left(x\frac{\partial}{\partial x}E_{zm}^{(1)}\right)+x\left(1-\frac{m^2}{x^2}\right)E_{zm}^{(1)}\right]$$
$$=\frac{4\pi}{\omega}\left\{-j_{zm}\alpha_{z1}^0 S_1-\frac{1}{\rho}\frac{\partial}{\partial\rho}(\rho j_{\theta m})-\frac{im}{\rho}j_{rm}+i\alpha_{x1}^0\left[\frac{1}{\rho}\frac{\partial}{\partial\rho}(\rho j_{rm})-\frac{im}{\rho}j_{\theta m}\right]\right\}, \tag{A 11}$$

where $x=\rho S_1$. One needs to find finite solutions of (A 11) which vanish at large radial distances from the beam axis, due to the fact that the source of the field is localized in the perpendicular direction; without a source term, a localized non-vanishing solution of (A 11) does not exist. The solutions can be expressed as the convolution of the right-hand side of (A 11) with a Green function which is constructed using two independent solutions of the corresponding Bessel equation (A 11) (that is, the Bessel function $J_m(x)$ of order m and the Hankel function $H_m^{(j)}(x)$ of order m and kind j) and satisfies to the necessary boundary conditions. Let us rewrite (A 11) for any j as

$$\frac{\partial}{\partial x}\left(x\frac{\partial}{\partial x}E_{zm}^{(j)}\right)+x\left(1-\frac{m^2}{x^2}\right)E_{zm}^{(j)}=-f^{(j)}(x), \tag{A 12}$$

which leads to

$$E_{zm}^{(j)}(x)=\int_0^\infty f^{(j)}(\xi)G_{(j)}(\xi,x)\,d\xi, \tag{A 13}$$

where the Green function $G_{(j)}(\xi,x)$ is defined by

$$G_{(j)}(\xi,x)=-\frac{i\pi}{2}(-1)^j\begin{cases}J_m(\xi)H_m^{(j)}(x), & \xi\leqslant x\\ J_m(x)H_m^{(j)}(\xi), & \xi\geqslant x\end{cases}. \tag{A 14}$$

In the case of electron whistler waves, the kind j of the Hankel function $H_m^{(j)}(x_j=\rho S_j)$ can be selected so that in a lossy plasma one has $\mathrm{Im}(S_2)<0$ for $\mathrm{Re}(S_2)>0$ (see, for example, [18]). The corresponding fields' components then vanish exponentially far away from the localized current system; for electron whistler waves the value $j=2$ corresponds to the largest root: $S_2^2>S_1^2$.

Integrating (A 13) by parts and taking into account (A 14) one gets

$$E_{zm}^{(j)}(x)=\frac{(-1)^{j+1}}{(b_2-b_1)}\int_0^\infty\frac{\xi d\xi}{S_j}\frac{4\pi}{\omega}\left[\left(-j_{zm}\alpha_{zj}^0+\frac{m}{\xi}\left(\alpha_{xj}^0 j_{\theta m}-ij_{rm}\right)\right)G_{(j)}(\xi,x)\right.$$
$$\left.+\left(j_{\theta m}-i\alpha_{xj}^0 j_{rm}\right)\mathbb{G}_{(j)}(\xi,x)\right], \tag{A 15}$$

with

$$\mathbb{G}_{(j)}(\xi,x)=-\frac{i\pi}{2}(-1)^j\begin{cases}J_m'(\xi)H_m^{(j)}(x), & \xi\leqslant x\\ J_m(x)H_m^{(j)\prime}(\xi), & \xi\geqslant x\end{cases}, \tag{A 16}$$

where $J_m'(\xi)$ and $H_m^{(j)\prime}(\xi)$ are the derivatives of the Bessel and the Hankel functions, respectively. One can express the other components of the electric field in the same way, which finally leads to the expressions (2)–(6).

https://doi.org/10.1017/S002237780500379X Published online by Cambridge University Press

The electromagnetic potentials $\mathbf{A}_m^{(j)}$ and $\Phi_m^{(j)}$ corresponding to the fields' expressions (2)–(6) can be written in the same manner as $\mathbf{E}_m^{(j)}$ as a function of $\mathscr{E}_m^{(j)}$ using

$$\mathscr{A}_m^{(j)}(x) = \frac{c}{\omega}\begin{bmatrix} -i\dfrac{m}{x}J_m(x) - i(\alpha_{xj}/\cos\phi_j)\cos^2\phi_j J'_m(x) \\ -(\alpha_{xj}/\cos\phi_j)\cos^2\phi_j \dfrac{m}{x}J_m(x) - J'_m(x) \\ -(\alpha_{xj}/\cos\phi_j)\sin\phi_j\cos\phi_j J_m(x) \end{bmatrix}, \tag{A 17}$$

and

$$\Phi_m^{(j)}(x) = -\frac{\alpha_{zj}}{k_j}J_m(x), \tag{A 18}$$

where $\cos\phi_j = k_z/k_j$.

Let us mention that the kind j of the Hankel function coincides with the numeration of the roots $k_{\perp j}$ only if $\mathrm{Im}(k_{\perp 1}) > 0$ and $\mathrm{Im}(k_{\perp 2}) < 0$ for $\mathrm{Re}(k_{\perp j}) > 0$ in a lossy plasma; for the electron whistler waves in a weakly lossy plasma, one has $|k_{\perp 1}| < |k_{\perp 2}|$ and near the branch $j = 2$ the transverse group velocity is directed opposite to the transverse wavevector.

The perpendicular field components can be obtained by substituting the expressions of the parallel fields $\bar{E}_z^{(j)}$ and $\bar{B}_z^{(j)}$ inside the following relations

$$\bar{B}_\theta = \frac{N_z^2\eta}{\varepsilon S_2^2 S_1^2}\frac{4\pi}{\omega}\left[\frac{i}{N_z}(N_z^2-\varepsilon)\bar{j}_\mathrm{r} - \frac{g}{N_z}\bar{j}_\theta\right] + \sum_{j=1,2}\left[\frac{ib_j N_z}{S_j^2}\frac{1}{\rho}\frac{\partial\bar{E}_z^{(j)}}{\partial\theta} + \frac{i\eta}{S_j^2}\frac{\partial\bar{E}_z^{(j)}}{\partial\rho}\right], \tag{A 19}$$

$$\bar{B}_\mathrm{r} = \frac{N_z^2\eta}{\varepsilon S_2^2 S_1^2}\frac{4\pi}{\omega}\left[-\frac{i}{N_z}(N_z^2-\varepsilon)\bar{j}_\theta - \frac{g}{N_z}\bar{j}_\mathrm{r}\right] + \sum_{j=1,2}\left[\frac{ib_j N_z}{S_j^2}\frac{\partial\bar{E}_z^{(j)}}{\partial\rho} - \frac{i\eta}{S_j^2}\frac{1}{\rho}\frac{\partial\bar{E}_z^{(j)}}{\partial\theta}\right], \tag{A 20}$$

$$\bar{E}_\mathrm{r} = \frac{N_z\eta}{\varepsilon S_2^2 S_1^2}\frac{4\pi}{\omega}\left[\frac{i}{N_z}(N_z^2-\varepsilon)\bar{j}_\mathrm{r} - \frac{g}{N_z}\bar{j}_\theta\right] + \sum_{j=1,2}\left[\frac{ib_j}{S_j^2}\frac{1}{\rho}\frac{\partial\bar{E}_z^{(j)}}{\partial\theta} + \frac{S_j^2-\eta}{iN_z S_j^2}\frac{\partial\bar{E}_z^{(j)}}{\partial\rho}\right], \tag{A 21}$$

$$\bar{E}_\theta = \frac{N_z\eta}{\varepsilon S_2^2 S_1^2}\frac{4\pi}{\omega}\left[\frac{i}{N_z}(N_z^2-\varepsilon)\bar{j}_\theta + \frac{g}{N_z}\bar{j}_\mathrm{r}\right] + \sum_{j=1,2}\left[-\frac{ib_j}{S_j^2}\frac{\partial\bar{E}_z^{(j)}}{\partial\rho} + \frac{S_j^2-\eta}{iN_z S_j^2}\frac{1}{\rho}\frac{\partial\bar{E}_z^{(j)}}{\partial\theta}\right]. \tag{A 22}$$

It is possible to show that (A19) can be simplified as

$$\bar{B}_\theta = \sum_{j=1,2}\left[\frac{ib_j N_z}{S_j^2}\frac{1}{\rho}\frac{\partial\bar{E}_z^{(j)}}{\partial\theta} + \frac{i\eta}{S_j^2}\frac{\partial\bar{E}_z^{(j)}}{\partial\rho}\right], \tag{A 23}$$

where the derivative of $\bar{E}_z^{(j)}$ over ρ in (A 23) should be understood as applied to the Green function terms under the integrals in (A 15) only. It is an essential and non-trivial simplification that in (A 23) one should not differentiate over the variable boundaries of the integrals, as it is necessary to do in (A 19) due to the different presentations of the Green function in the different domains of its arguments (see (A 13) and (A 14)).

https://doi.org/10.1017/S002237780500379X Published online by Cambridge University Press

Similar formulas can be found for the other field components, i.e. the terms in $\bar{B}_\mathrm{r}$ and $\bar{E}_\theta$ containing the current density will be eliminated in (A 20) and (A 22); however, as mentioned above, the derivatives over ρ should be only applied to the terms under the integrals which are connected to the Green functions. For the radial electric field, one has

$$\bar{E}_\mathrm{r} = \frac{4\pi}{\omega}\left(-\frac{i}{\varepsilon}\right)\bar{j}_\mathrm{r} + \sum_{j=1,2}\left[\frac{ib_j}{S_j^2}\frac{1}{\rho}\frac{\partial \bar{E}_z^{(j)}}{\partial\theta} + \frac{S_j^2-\eta}{iN_z S_j^2}\frac{\partial \bar{E}_z^{(j)}}{\partial\rho}\right], \tag{A 24}$$

where $\bar{j}_\mathrm{r} = 0$ for the case of coaxial beam particles' motion (with the axis of the cylindric reference frame coinciding with the beam axis).

Appendix B. Numeration of the waves' branches

In a cold homogeneous magnetized and weakly lossy plasma, it is possible to show that the sign of the small imaginary part of the perpendicular wave number is adjusted to the sign of the perpendicular group velocity as follows (using [53])

$$2\mathrm{Re}(k_{\perp 1})\mathrm{Im}(k_{\perp 1}) = \frac{\omega^2}{c^2}\mathrm{Im}(N_1^2(\omega,\phi_1))\frac{(1+\alpha_{x1}^2)}{(S_1^2-S_2^2)}\frac{g\eta}{\varepsilon}\frac{\cos\phi_1}{\alpha_{x1}} > 0,$$

$$\mathrm{Re}(k_{\perp 1}) > 0, \quad j = 1, \tag{B 1}$$

where the parameter $\cos\phi_j/\alpha_{xj}$ keeps its sign (negative for the electron sense of polarization) independently on the sign of $\cos\phi_j$. For whistlers in a dense plasma one has $\cos\phi_j/\alpha_{xj} \approx -|\cos\phi_j|$. On the other hand

$$(\mathbf{k}_\perp \cdot \mathbf{v}_{g\perp})_1 = 2\omega S_1^2\frac{\varepsilon}{g\eta}\frac{\alpha_{x1}}{\cos\phi_1}\frac{(S_1^2-S_2^2)}{(1+\alpha_{x1}^2)}\left[\frac{\partial}{\omega\partial\omega}\omega^2\mathrm{Re}N_1^2(\omega,\phi_1)\right]^{-1}$$

$$= \omega S_1^2\frac{\omega^2}{c^2}\frac{\mathrm{Im}(N_1^2(\omega,\phi_1))}{\mathrm{Re}(k_{\perp 1})\mathrm{Im}(k_{\perp 1})}\left[\frac{\partial}{\omega\partial\omega}\omega^2\mathrm{Re}N_1^2(\omega,\phi_1)\right]^{-1}, \tag{B 2}$$

where the term of (B 2) in the square brackets is positive for the positive energy waves ($\partial\omega^2\mathrm{Re}N^2(\omega,\phi)/\partial\omega > 0$), which proves that for positive values of $\mathrm{Im}(k_{\perp 1})$ the perpendicular group velocity and the perpendicular wave vector have the same direction; note that it is not the case for the branch $j = 2$ (in (B 1) one should replace the index 1 by the index 2).

Considering under the same conditions the equation for the growth rate γ of a plane wave

$$\frac{\partial\omega^2\mathrm{Re}(N^2(\omega,\phi))}{\partial\omega}\gamma + \mathrm{Im}(N^2(\omega,\phi)) = 0, \tag{B 3}$$

one can see that the sign of $\mathrm{Im}(N^2(\omega,\phi))$ in a weakly lossy plasma should be positive for waves of positive energy, so that the wave is absorbed ($\gamma < 0$). Thus one has

$$\frac{1}{(S_1^2-S_2^2)}\frac{g\eta}{\varepsilon}\frac{\cos\phi_1}{\alpha_{x1}} > 0, \tag{B 4}$$

with the following direct consequence for electron whistlers in a dense plasma: $(S_1^2-S_2^2) < 0$.

https://doi.org/10.1017/S002237780500379X Published online by Cambridge University Press

Appendix C. Beam particles' motion

For a quasi-coaxial beam with small scattering of its parallel particles' velocities near v_{bz} (16), the equations of particles' motion in the field (1) can be written in a rather general form as

$$\frac{dv_z}{dt} = -\frac{\omega_c}{2} hW \exp(i\eta) + \text{c.c.}, \tag{C 1}$$

$$\frac{dv_\perp}{dt} = \frac{d\theta}{dt}\frac{dr}{dt} + r\frac{d^2\theta}{dt^2} = -\frac{\omega_c}{2v_\perp} hK \exp(i\eta) + \text{c.c.}, \tag{C 2}$$

$$\frac{d^2\eta_p}{dt^2} = k_z \frac{dv_{zp}}{dt} - \frac{m\omega_c}{v_{\perp p}}\frac{dv_{\perp p}}{dt} \simeq -k_z \frac{\omega_c}{2}\left(1 + \frac{m^2\omega_c^2}{v_{\perp p}^2}\right) e^{i\eta_p} \sum_{j=1}^{2} h_j W_j(x_{jp}) + \text{c.c.}, \tag{C 3}$$

with

$$hW \equiv \sum_{j=1,2} h_j W_j(x_j), \quad hK \equiv \sum_{j=1,2} h_j K_j(v_z, x_j), \tag{C 4}$$

where h_j corresponds to the normalized contribution of the whistler branch j to the effective field excited by the beam (R is the radial size of the cylindrical tube containing the beam)

$$h_j = \pi \frac{4\pi e}{c^2}\frac{k_z}{m_e\omega_c}\frac{g\eta}{\varepsilon}\frac{1}{\sigma_j(S_2^2 - S_1^2)}\int_0^R r' dr' \mathscr{P}_m^{(j)}(k_{\perp j} r'). \tag{C 5}$$

The functions $W_j(x_j)$ and $K_j(v_z, x_j)$ are defined as

$$\begin{aligned} x_j > x_j', \quad W_j(x_j) \equiv W_j^{\mathrm{H}}(x_j) &= -v_{bz}\alpha_{zj}^0 H_m^{(j)}(x_j) \\ &\quad + v_\perp\left[\frac{m}{x_j}\alpha_{xj}^0 H_m^{(j)}(x_j) + H_m^{(j)'}(x_j)\right], \\ x_j' > x_j, \quad W_j(x_j) \equiv W_j^{\mathrm{B}}(x_j) &= -v_{bz}\alpha_{zj}^0 J_m(x_j) + v_\perp\left[\frac{m}{x_j}\alpha_{xj}^0 J_m(x_j) + J_m'(x_j)\right], \end{aligned} \tag{C 6}$$

$$\begin{aligned} x_j > x_j', \quad K_j(v_z, x_j) &= -\left(\frac{m\omega_c}{k_z} + u\right) W_j^{\mathrm{H}}(x_j) - u\alpha_{zj}^0 \frac{\omega}{k_z} H_m^{(j)}(x_j), \\ x_j' > x_j, \quad K_j(v_z, x_j) &= -\left(\frac{m\omega_c}{k_z} + u\right) W_j^{\mathrm{B}}(x_j) - u\alpha_{zj}^0 \frac{\omega}{k_z} J_m(x_j), \end{aligned} \tag{C 7}$$

where $u = v_z - v_{bz}$, $x_j = k_{\perp j} r = \rho S_j$ and $x_j' = k_{\perp j} r'$. Then, in the right-hand side of the particles' motion equation (C 3), for example, one can present $h_j W_j(x_j)$ in the following form

$$h_j W_j(x_j) = -\left|\frac{2\pi e I_b}{m_e c^3}\right| \frac{c}{|v_{bz}|}\frac{k_z}{\omega_c}\left(\frac{g\eta}{\varepsilon}\right)\frac{1}{\sigma_j}\frac{W_j(x_j)}{(S_2^2 - S_1^2)}\int_0^T \frac{dt}{T}\frac{1}{N_p}\sum_{p=1}^{N_p} W_j(k_{\perp j} r_p) e^{-i\eta_p}. \tag{C 8}$$

References

[1] Shapiro, V. D. and Shevchenko, V. I. 1971 Contribution to the nonlinear theory of relaxation of a monoenergetic beam in a plasma. *Sov. Phys.–JETP* **33**, 555.

[2] O'Neil, T. M., Winfrey, J. H. and Malmberg, J. H. 1971 Nonlinear interaction of a small cold beam and a plasma. *Phys. Fluids* **14**, 1204.

https://doi.org/10.1017/S002237780500379X Published online by Cambridge University Press

[3] Matsiborko, N. G., Onishchenko, I. N., Shapiro, V. D. and Shevchenko, V. I. 1972 Of nonlinear theory of instability of a mono-energetic electron beam in plasma. *Plasma Phys.* **14**, 1204.

[4] Ivanov, A. A., Parail, V. V. and Soboleva, T. K. 1973 Nonlinear theory of the interaction between a monoenergetic beam and a dense plasma. *Sov. Phys.–JETP* **36**, 887.

[5] Singh, R. P. 1973 Cherenkov-cyclotron power generated in the magnetosphere by natural and artificial injection of electron beams. *Ann. Geophys.* **29**, 227.

[6] Matsumoto, H. and Yasuda, Y. 1976 Computer simulation of nonlinear interaction between a monochromatic whistler wave and an electron beam. *Phys. Fluids* **19**, 1513.

[7] Matsumoto, H., Hashimoto, K. and Kimura, I. 1980 Dependence of coherent nonlinear whistler interaction on wave amplitude. *J. Geophys. Res.* **85**, 644.

[8] Le Quéau, D., Pellat, R. and Saint Marc, A. 1981 Electrostatic instabilities of a finite electron beam propagating in a cold magnetized plasma. *Phys. Rev. A* **24**, 448.

[9] Lavergnat, J., Le Quéau, D., Pellat, R. and Roux, A. 1982 Nonlinear radiation by an electron beam in the whistler range: A tentative theoretical model. *Phys. Fluids* **25**, 1073.

[10] Omura, Y. and Matsumoto, H. 1982 Computer simulations of basic processes of coherent whistler wave-particles interactions in the magnetosphere. *J. Geophys. Res.* **87**, 4435.

[11] Omura, Y. and Matsumoto, H. 1987 Competing processes of whistler and electrostatic instabilities in the magnetosphere. *J. Geophys. Res.* **92**, 8649.

[12] Kovalenko, V. P. 1983 Electron bunches in nonlinear collective beam-plasma interaction. *Sov. Phys. Usp.* **26**, 116.

[13] Harker, K. J. and Banks, P. M. 1983 Radiation from pulsed electron beams in space plasmas. *Radio Sci.* **19**, 454.

[14] Harker, K. J. and Banks, P. M. 1987 Near fields in the vicinity of pulsed electron beam in space. *Planet. Space Sci.* **35**, 11.

[15] Nishikawa, K. I., Frank, L. A. and Huang, C. Y. 1989 Three-dimensional simulation of whistler mode excited by the Spacelab 2 electron beam. *J. Geophys. Res.* **94**, 6855.

[16] Nishikawa, K. I., Buneman, O. and Neubert, T. 1994 New aspects of whistler waves driven by an electron beam studied by a 3D electromagnetic code. *J. Geophys. Res.* **94**, 6855.

[17] Zhang, Y. L., Matsumoto, H. and Omura, Y. 1993 Linear and nonlinear interactions of an electron beam with oblique whistler and electrostatic waves in the magnetosphere. *J. Geophys. Res.* **98**, 21 353.

[18] Lundin, B., Chmyrev, V., Krafft, C. and Matthieussent, G. 1994 VLF emission produced by a rarefied electron beam during active experiments in the Earth ionosphere: Conditions of observation of the emission. *J. Geophys. Res.* **99**, 14 987.

[19] Lundin, B., Krafft, C. and Matthieussent, G. 1995 Whistler emissions produced by modulated electron beams injected into the ionosphere. *J. Geophys. Res.* **100**, 3703.

[20] Pivovarov, V., Burke, A., Ride, S. K. and Shapiro, V. D. 1995 Excitation of VLF waves by an electron beam injected into the ionosphere. *J. Geophys. Res.* **17**, 17 515.

[21] Lundin, B. and Krafft, C. 1999 Emission of a bounded nonmonoenergetic electron beam injected in the ionosphere. *J. Geophys. Res.* **104**, 143.

[22] Volokitin, A., Krafft, C. and Matthieussent, G. 1997 Whistler waves emission by a modulated electron beam: Nonlinear theory. *Phys. Plasmas* **4**, 4126.

[23] Volokitin, A. and Krafft, C. 2000 Dynamically stable electron bunches in beam interaction with an electromagnetic wave packet. *JETP Lett.* **71**, 262.

[24] Volokitin, A. and Krafft, C. 2001a Electron beam interaction with lower hybrid waves at Cherenkov and cyclotron resonances. *Phys. Plasmas* **8**, 3748.

[25] Volokitin, A. and Krafft, C. 2001b Spiral electron beam interaction with whistler waves at cyclotron resonances. *Phys. Plasmas* **8**, 4960.

[26] Krafft, C., Volokitin, A. and Flé, M. 2000 Nonlinear electron beam interaction with a whistler wave packet. *Phys. Plasmas* **7**, 4423.

https://doi.org/10.1017/S002237780500379X Published online by Cambridge University Press

[27] Krafft, C. and Volokitin, A. 1998 Nonlinear interaction of whistler waves with a modulated thin electron beam. *Phys. Plasmas* **5**, 4243.

[28] Krafft, C. and Volokitin, A. 2002 Resonant electron beam interaction with several lower hybrid waves. *Phys. Plasmas* **9**, 2786.

[29] Krafft, C. and Volokitin, A. 2003 Interaction of a wave packet with a thin electron beam spiraling in a magnetized plasma. *Phys. Plasmas* **10**, 3093.

[30] Cartwright, D. R. and Kellogg, P. J. 1974 Observations of radiation from an electron beam artificially injected into the ionosphere. *J. Geophys. Res.* **79**, 1439.

[31] Winckler, J. R. 1980 The applications of artificial electron beams to magnetospheric research. *Rev. Geophys. Space Phys.* **18**, 659.

[32] Winckler, J. R. 1992 Controlled experiments in the Earth's magnetosphere with artificial electron beams. *Rev. Mod. Phys.* **64**, 859.

[33] Lin, R. P., Potter, D. W., Gurnett, D. A. and Scarf, F. L. 1981 Energetic electrons and plasma waves associated with a solar type III radio burst. *Astrophys. J.* **251**, 364.

[34] Kellogg, P. J., Monson, S. J., Bernstein, W. and Whalen, B. A. 1986 Observation of waves generated by electron beams in the ionosphere. *J. Geophys. Res.* **91**, 12 065.

[35] Lavergnat, J. 1982 The French–Soviet experiment ARAKS: Main results. In *Artificial Particle Beams in Space Plasmas Studies* (ed. Grandal, B.). New York: Plenum Press, p. 87.

[36] Farrell, W. M., Gurnett, D. A. and Goertz, C. K. 1989 Coherent Cherenkov radiation from the Spacelab 2 electron beam. *J. Geophys. Res.* **94**, 443.

[37] Nemzek, R. J. and Winckler, J. R. 1991 Electron beam sounding rocket experiments for probing the distant magnetosphere. *Phys. Rev. Lett.* **67**, 987.

[38] Neubert, T. and Banks, P. M. 1992 Recent results from studies of electron beam phenomena in space plasmas. *Planet. Space Sci.* **40**, 153.

[39] Stenzel, R. L. and Golubyatnikov, G. 1993 Cyclotron harmonic lines in the thermal magnetic fluctuations spectrum of spiraling electrons in plasmas. *Phys. Fluids B* **5**, 3789.

[40] Oraevsky, V. N. et al. 1994 Effects of artificially injected electron beams on the characteristics of ground VLF transmitter signals in the ionosphere. *J. Atmos. Terrest. Phys.* **56**, 423.

[41] Thejappa, G., Wentzel, Donat G. and Stone, R. G. 1995 Low-frequency waves associated with Langmuir waves in solar wind. *J. Geophys. Res.* **100**, 3417.

[42] Raitt, W. J. 1996 Active plasma experiments in space: Steps toward a space laboratory facility. In *Review Radio Science 1993–1996* (ed. Ross Stone, W.). Oxford: Oxford University Press, p. 651.

[43] Miller, J. A., Cargill, P. J., Emslie, A. G., Holman, G. D., Dennis, B. R., LaRosa, T. N., Winglee, R. M., Benka, S. G. and Tsuneta, S. 1997 Critical issues for understanding particle acceleration in impulsive solar flares. *J. Geophys. Res.* **102**, 14 631.

[44] Dulk, G. A., Leblanc, Y., Robinson, P. A., Bougeret, J. L. and Lin, R. P. 1998 Electron beams and radio waves of solar type III bursts. *J. Geophys. Res.* **103**, 17 223.

[45] Moullard, O., Burgess, D. and Bale, S. D. 1998 Whistler waves observed during an in-situ solar type III radio burst. *Astron. Astrophys.* **335**, 703.

[46] Ergun, R. E. et al. 1998 Wind spacecraft observations of solar impulsive electron events associated with solar type III radio bursts. *Astrophys. J.* **503**, 435.

[47] Stenzel, R. L. 1999 Whistler waves in space and laboratory plasmas. *J. Geophys.Res.* **104**, 14 379.

[48] Krafft, C. and Starodubtsev, M. 2002 Whistler excitation by electron beams in laboratory plasmas. *Planet. Space Sci.* **50**, 129.

[49] Muschietti, L., Roth, I. and Delory, G. 1997 Oblique turbulence driven by field-aligned electron fluxes in the auroral ionosphere. *J. Geophys. Res.* **102**, A12, 27 217.

[50] Garnett, D. A. 1974 The Earth as a radio source: Terrestrial kilometric radiation. *J. Geophys. Res.* **79**, 4227.

https://doi.org/10.1017/S002237780500379X Published online by Cambridge University Press

[51] Allis, W. P., Buchsbaum, S. J. and Bers, A. 1963 *Waves in Anisotropic Plasmas*. Cambridge, MA: MIT Press.

[52] Kondrat'ev, I. G., Kudrin, A. V. and Zaboronkova, T. M. 1999 *Electrodynamics of Density Ducts in Magnetized Plasmas*. Gordon and Breach Science Publishers.

[53] Shafranov, V. D. 1967 *Electromagnetic Waves in Plasma*. In: Reviews of plasma physics, Vol. 3 (ed. Leontovich, M. A.). New York: Consultants Bureau, p. 1.

[54] Abramovitz, M. and Stegun, I. A. 2000 *Handbook of Mathematical Functions*. New York: Dover.

[55] Lundin, B. and Krafft, C. 2002 Modified electron whistler dispersion law. *J. Plasma Phys*. **67**, 149.

[56] Reynolds, M. A. and Morales, G. J. 1996 High-frequency fluctuations of a modulated, helical electron beam. *Phys. Plasmas* **3**, 4717.

[57] Wieder, B. 1964 Microwave propagation in an overdense bounded magnetoplasma. *Phys. Fluids* **7**, 964.

https://doi.org/10.1017/S002237780500379X Published online by Cambridge University Press